Physical models for the 21cm Emission and Absorption spectra from the Galactic Interstellar Medium

A thesis submitted towards partial fulfilment of
BS-MS Dual Degree Programme

by

Tushar Sanjay Shrotriya

under the guidance of

Jayaram Chengalur

National Centre for Radio Astrophysics (NCRA),
TIFR, Pune

Indian Institute of Science Education and Research
Pune

Certificate

This is to certify that this thesis entitled "Physical models for the 21cm Emission and Absorption spectra from the Galactic Interstellar Medium" submitted towards the partial fulfilment of the BS-MS dual degree programme at the Indian Institute of Science Education and Research Pune represents original research carried out by Tushar Sanjay Shrotriya at National Centre for Radio Astrophysics (NCRA), TIFR, Pune, under the supervision of Jayaram Chengalur during the academic year 2012-2013.

Student
Tushar Sanjay
Shrotriya

Supervisor
Jayaram
Chengalur

Acknowledgements

I would like to thank my mentor, Jayaram Chengalur and my TAC member, Nissim Kanekar, for their constant support and guidance throughout the duration of the project. I would also like to thank NCRA for allowing me to use their facilities for the duration of this project. I would like to thank my local co-ordinator, Ramana Athreya, for the moral support he gave when I needed it. And finally I would like to thank IISER for everything.

Abstract

Understanding the Interstellar Medium (ISM) is crucial to understand the structure, formation and dynamics of a galaxy. Interstellar HI provides a great probe of the ISM and high quality data are constantly being produced by the best radio telescopes. Analyzing this data can provide great insights for understanding our galaxy. However, so far, we have been limited in interpreting the high quality data. We here work with some high quality absorption and emission spectra and using a special solution of the radiative transfer equation, we try to fit the spectra jointly with our model. A C-based version of Minuit (a minimization algorithm maintained by scientists at the CERN lab) was used to minimize the χ^2 and obtain good fits to the data. With the radiative transfer equation taken into account, the spatial ordering built into the model and a multiparameter fitting routine with all parameters free, our model is a new approach to dealing with this problem and is likely to be useful for analyzing the data in the future. Using our model, we can use the spectra to describe sight-lines in detail and estimate the distribution of the interstellar HI into three types of components - Cold Neutral Medium (40-200 K), Warm Neutral Medium (>5000 K) and thermally unstable medium (500-5000 K) - in the direction of the sight-lines. We have described 3 such sight-lines - PKS 0407-658, 3C286 and PKS 1814-637. PKS 0407-658 could be fit with 11 components and is estimated to have $69.9 \pm 6.4\%$ of the N_{HI} in the WNM, $16.7 \pm 1.0\%$ in the CNM and $13.5 \pm 2.1\%$ in the unstable medium. 3C286 could be fit with 6 components and is estimated to have $74 \pm 36\%$ of the N_{HI} in the WNM, $12.9 \pm 2.1\%$ in the CNM and $13 \pm 16\%$ in the unstable medium. PKS 1814-637 could be fit with 8 components and is estimated to have $26.0 \pm 2.1\%$ of the N_{HI} in the WNM, $21.0 \pm 1.6\%$ in the CNM and $52.9 \pm 2.1\%$ in the unstable medium.

Contents

Chapter 1

Introduction

HI studies continue to be really important for the study of the Galaxy because of high quality emission and absorption data made continuously available by various radio telescopes all over the world. These studies particularly focus on a hyperfine structure spin-flip transition line of neutral hydrogen which has a wavelength of around 21 cm and a frequency of around 1420 Mhz. This line lies in the radio region, to which our atmosphere and most of the interstellar medium is transparent. This makes the observations of interstellar HI an effective tool of measuring the presence of Hydrogen, the most abundant element in the universe.

Analyzing the available data can give great information about the interstellar medium (ISM), which in turn, is of great importance to understand our galaxy better. One particular way in which this can be done is the analysis of absorption and emission spectra by fitting them with model spectra. Starting from first principles of radiative transfer, we build our model to fit the absorption and emission spectra jointly, which enables us to physically interpret the structure of the ISM visible in the spectra.

1.1 The Interstellar Medium

The interstellar medium in our galaxy consists majorly of neutral hydrogen (HI), ionised hydrogen (HII), molecular hydrogen (H_2) and dust. Interstellar HI in our galaxy is believed to contribute about 4.8×10^9 $M_\odot$, which is 4.4% of the visible matter of the galaxy and it has a filling factor, the exact value of which remains uncertain, between 20% and 90%.[1] Because HI is a major component of the ISM of the Galaxy, many observational studies have focused on HI and high quality data are being constantly produced.

1.2 The 21 cm HI line

One of the best indicators of the presence of HI in the interstellar medium is the 21 cm spin-flip transition line of HI. This transition occurs when the electron and proton change states from having parallel spins to having antiparallel spins, which has a little lower energy and the energy is emitted in the form of a 21 cm wavelength photon. This spontaneous emission has an extremely low Einstein coefficient of around 2.85×10^{-15} s^{-1} which gives it a half-life of A$^{-1} \approx 12$ million years. But the sheer number of hydrogen atoms in the galaxy leads to strong radio emission from all sight-lines.[1]

1.3 Radiative Transfer

Consider a ray of light with intensity I_ν passing through a region of length ds inside a cloud with emission coefficient j_ν and absorption coefficient α_ν. The change in the intensity dI_ν is given by

$$dI_\nu = j_\nu ds - \alpha_\nu I_\nu ds \tag{1.1}$$

Now $\alpha_\nu ds$ is the change in the optical depth $d\tau_\nu$. Replacing that into Eq. 1.1 and dividing by $d\tau_\nu$, we get

$$\frac{dI_\nu}{d\tau_\nu} = \frac{j_\nu}{\alpha_\nu} - I_\nu \tag{1.2}$$

Now, under conditions of equilibrium at temperature T, $dI_\nu = 0$, meaning that

$$\frac{j_\nu}{\alpha_\nu} = I_\nu = B_\nu(T) \tag{1.3}$$

where $B_\nu(T)$ is the Planck spectrum at temperature T. So, Eq. 1.2 becomes

$$\frac{dI_\nu}{d\tau_\nu} = B_\nu(T) - I_\nu \tag{1.4}$$

Now, if $h\nu \ll kT$, which is in fact the case for the radio frequencies, we can use the Rayleigh-Jeans law and get the brightness temperature

$$T_{B,\nu} = \frac{c^2 I_\nu}{2\nu^2 k} \tag{1.5}$$

In general one can define $T_{B,\nu}$ by the above relation even when the radiation is not characterized by the Planck spectrum. Also the spin temperature for the 21 cm line is defined by

$$e^{-\frac{h\nu}{kT_S}} = \frac{g_1 n_2}{g_2 n_1} \tag{1.6}$$

where n_1 and n_2 are the populations at the lower and upper hyperfine states, respectively and $g_2 = 3$ and $g_1 = 1$ are the statistical weights of the hyperfine states. Using this definition of spin temperature and Eq. 1.5, we get

$$\frac{dT_{B,\nu}}{d\tau_\nu} = T_S - T_{B,\nu} \tag{1.7}$$

This is the radiative transfer equation that is used most often in radio astronomy. Of particular interest to us is a special solution for this equation which assumes that the radiation is passing through a uniform isothermal cloud:

$$T_{B,\nu} = T_{bg,\nu}e^{-\tau_\nu} + T_S(1 - e^{-\tau_\nu}) \tag{1.8}$$

where T_{bg} is the brightness temperature of the background radiation.[2]

Note that the frequency in the above equations can be replaced by the equivalent velocity for small values of velocity due to the Doppler shift in frequency that is linear in velocity. This approximation holds for all of our sight-lines and we will deal with velocities in all further analysis. We also assume that the velocities follow a Maxwellian distribution, meaning that the spectral lines are broadened thermally and have Gaussian profiles.

1.4 General Case with N clouds

Let us consider a general case with N uniform isothermal clouds, where the clouds are numbered in the order in which the radiation passes through them (i.e. the farthest cloud is cloud 1 and the nearest cloud is cloud N). For such a case, the expression for the optical depth is

$$\tau(v) = \sum_{i=1}^{N} \tau_i(v) \tag{1.9}$$

where $\tau_i(v)$ is the optical depth of the i^{th} cloud. The brightness temperature after the ray passes the i^{th} cloud can be expressed using Eq. 1.8 as

$$T_{B,i}(v) = T_{B,i-1}(v)e^{-\tau_i(v)} + T_{S,i}(1 - e^{-\tau_i(v)}) \tag{1.10}$$

where $T_{S,i}$ is the spin temperature of the i^{th} cloud and $T_{B,0} = T_{bg} = 0$. The final brightness temperature, $T_{B,N}(v)$, can be obtained by iteratively calculating the brightness temperatures starting from the first cloud till the N^{th} cloud. This can be expressed as

$$T_{B,N}(v) = \sum_{i=1}^{N} \left[T_{S,i} \left(1 - e^{-\tau_i(v)}\right) \right] \exp\left(- \sum_{j=i+1}^{N} \tau_j(v) \right) \tag{1.11}$$

1.4.1 Optically Thin Limit

In the optically thin limit ($\tau \ll 1$), Eq. 1.8 modifies to give

$$T_B(v) = T_{bg}(v)(1 - \tau(v)) + T_S\tau(v) \tag{1.12}$$

This special case allows for the brightness temperatures to be additive if you have more than one isothermal cloud and if $T_{bg} \ll T_S$ which is almost always the case. For instance, for a case of N isolated isothermal clouds in the same line of sight and no background radiation,

$$T_B(v) = \sum_{i=1}^{N} T_{S,i}\tau_i(v) = \sum_{i=1}^{N} T_B^i(v) \tag{1.13}$$

This allows for modelling emission spectra where the optical depth is low as multiple superposed Gaussians. Such a model would not be physically motivated were the brightness temperatures not additive.

1.5 The Kinetic and Spin Temperatures of Interstellar HI

From Eq. 1.6, one can see that the spin temperature of HI is determined by the distribution of atoms in the energy levels of the 21cm line. The presence of the cosmic microwave background radiation of 2.73 K sets an absolute lower limit for the spin temperature. However, in almost all cases, the spin temperature is much higher than this limit. Under the case that the gas is in collisional equilibrium, which is often true for the cold dense gas clouds, the excitation is driven by collisions, which force the spin temperature to be equal to the kinetic temperature. This may not be true for the warmer, less dense gas phases and in such cases the spin temperature is less than the kinetic temperature, but never more.

Lyα excitation is another process which can determine the spin temperature, and plays an important role in systems where the number densities are low and collisions do not determine the spin temperature. An electron in the lower hyperfine state of the ground electronic state can get excited to a higher electronic state on absorbing a Lyman photon and lose another photon with a slightly smaller frequency and go back to the higher hyperfine state of the ground electronic state. The rate of effective excitation to the higher hyperfine state is determined by the difference in the intensities of the Lyα radiation at these frequencies. Since Lyα transition has a very high Einstein co-efficient, causing the electron to fall back to the ground state very fast,

almost all hydrogen atoms are in their ground electronic state. This means that the optical depth of the interstellar neutral hydrogen for Lyα radiation is very high. This leads to the photons getting absorbed and reemitted a large number of times before they escape a cloud. This, in turn, causes the Lyα line profile to flatten near the centre and gives it a slope of $\exp(-h\nu/kT_k)$. This causes the difference between the intensities at the two frequencies to be exactly that required for the spin temperature to be equal to the kinetic temperature. However, since Lyα photons have a high optical depth, they are unlikely to penetrate a cloud from outside and in many situations, the Lyα intensity may not be sufficient to drive the spin temperature to the kinetic temperature. Most situations in which Lyα radiation pushes the spin temperature towards kinetic temperature are those in which a source of Lyα photons such as a hot, bright star lies inside the HI region.[1]

1.6 Components of Interstellar HI

Traditionally, the interstellar HI is known to co-exist in two thermal equilibrium phases - the Cold and Warm Neutral Media. However, there is evidence for existence of a third thermally unstable medium which has temperatures in between those typical of the other two phases. The distribution of the interstellar HI among these three components remains uncertain. We try to estimate this distribution in this analysis.

1.6.1 Warm Neutral Medium

Almost half of all the HI in the galaxy is believed to be in the form of Warm Neutral Medium (WNM). WNM fills a substantial fraction of the ISM and is extensive and visible in all directions. It has low volume density ($\sim$0.1 atoms/cc) and has a kinetic temperature of $\sim$ 8,000 K (but this is just a rough estimate). WNM usually has low optical depth, but is visible in emission and has wide emission profiles corresponding to it.

1.6.2 Cold Neutral Medium

Embedded in the WNM are dense clouds of Cold Neutral Medium (CNM). They usually have a clumpy distribution across the galaxy. CNM has higher densities of around 10 atoms/cc and temperatures of around 80 K. The clouds tend to have a high optical depth and are visible both in absorption and emission as narrow profiles.[1]

1.6.3 Thermally Unstable Neutral Medium

Some of the Warm Neutral Medium is believed to be thermally unstable. The typical temperatures characterising thermally unstable warm medium are between 500 K and 5000 K. This medium is typically visible in both emission and absorption. The fraction of the neutral hydrogen in the unstable medium remains uncertain.[3, 4]

1.7 Previous Work

Heiles and Troland (2003)[5, 4] tried analyzing the absorption and emission spectra, and their approach was similar to what we initially tried. However, their models differ from our final model in many aspects.

They tried to fit the emission and absorption spectra with two kinds of components - those which are visible in emission and absorption (they classify them further as CNM and CNM-associated WNM depending on their kinetic temperatures) and those visibile in only the emission spectra (WNM). They first tried to fit the spectra jointly using Gaussians for both absorption and emission and then tried to shuffle the order of the components, now with the radiative transfer equation applied, to look for the best solution. Doing this leads to problems such as factorial order algorithms (see Sec. 4.2).

Also, the quality of the data we have available is much higher than what they had. Because the quality of data they had was not so good, they could work with approximate models and still get decent fits to the data. However, with the quality of data we have now, we require a more accurate, physically motivated model, which takes into account the radiative transfer equation, has spatial ordering built into the code and treats the CNM and WNM similarly.

They also arrived at the fractions of interstellar HI in the cold, warm and unstable media. They estimated that 60% of the gas lies in the warm and unstable neutral media, of which at least 48% (and hence at least 29% of the total HI) lies in the unstable medium. We compare our results with theirs later in Sec. 4.1.

Kanekar et. al. (2003)[3] also did a similar analysis, but with only the absorption spectra. They tried fitting Gaussians to the absorption profiles. From fits to two spectra (PKS 0407-658 and PKS 1814-637), they found that all the warm components visible in absorption had kinetic temperatures between 2000 K and 4000 K, meaning that they were all in the unstable neutral medium. However, the lack of emission data means that they could not estimate the fraction of total HI in the unstable phase.

Chapter 2

Methods

2.1 Data

2.1.1 How the spectra are generated

For the emission spectrum you measure the antenna temperature which corresponds to the brightness temperature of the ISM which is a measure of the intensity and for the long radio wavelengths $I_\nu = 2\nu^2 kT/c^2$.

For absorption, you choose a small, but bright background continuum source. The absorption is measured using interferometers where the contributions of the spatially smooth emission is largely "resolved" out.[3]

2.1.2 Emission Data - LAB Survey

The Leiden-Argentine-Bonn (LAB) Survey[6] is an all sky survey looking for 21 cm emission from all over the galaxy. It uses two telescope surveys - Leiden/Dwingeloo Survey (LDS)[7] on the Dwingeloo Telescope for the northern sky and Instituto Argentino de Radioastronomia Survey (IAR)[8, 9] on the Villa Elisa telescope for the southern sky. The improved stray radiation corrections, which they have a better control over in an all sky survey, allow them to improve the signal fidelity and provide high quality emission data.[6] Data from the Parkes telescope based GASS survey, which have better velocity resolution, is also available, but for the project, we have used the LAB spectra because of their better signal-to-noise ratio. The LAB data typically has an RMS noise of about 0.07-0.09 K, but we worked on two spectra with noise ~ 0.04 K (at a velocity resolution of 1.03 km/s). The data available from their database is truncated at the second decimal place, which, although does not make much difference with the analysis, causes the Anderson-Darling test to detect departures from normality of the noise due

to the truncation (see Sec. 2.3.2 for more details), but in the end we were able to get good fits without this problem.

2.1.3 Absorption Data

The 21 cm HI absorption data used in this project were obtained from observations with the Australia Telescope Compact Array (ATCA)[3] (for PKS 0407-658 and PKS 1814-637) and the Westerbork Synthesis Radio Telescope (WSRT)[10] (for 3C286). Data processing had already been done and the final absorption spectra were made available. The RMS noise in the optical depth was 0.001 at a velocity resolution of 0.4 km/s for the ATCA data and 0.0003 at a velocity resolution of 0.515 km/s for the WSRT data.

2.2 The Model

2.2.1 Gaussian Fitting

Spectral lines whose width is determined by thermal broadening tend to exhibit Gaussian line profiles. Since in the optically thin limit, the brightness temperature is just the spin temperature times the optical depth, both emission and absorption profiles are Gaussian and as a first approximation and a preliminary test, we started by trying to fit simple Gaussians to both emission and absorption spectra independently. However, fitting multiple Gaussians to a spectrum is not very straightforward as Gaussians form a non-orthogonal basis set (i.e. you can fit the same spectrum with different sets of Gaussians in different ways). This forces us to use the minimum number of Gaussians to fit the data, as you can always add more Gaussians and still be able to fit the data in multiple ways. So, the automated code would start with a single Gaussian and go on adding Gaussians till it found a fit good enough, which is determined using the reduced χ^2 and the Anderson-Darling Test Statistic (see Sec. 2.3.2).

2.2.2 Joint Fitting

Most components contributing to the absorption spectrum also contribute to the emission spectrum. However, some warmer components can have low enough optical depth, or can be absent from the absorption field of view, so that they are not visible in the absorption spectra. So we tried to fit both the emission and absorption spectra together using simple Gaussian components which are visible in both absorption and emission spectra as well as additional

Gaussian components which are only visible in the emission spectra, using a joint χ^2 statistic as the function to be minimized.

2.2.3 Spatial Ordering

As seen in the solution to the radiative transfer equation in the non-optically thin case (Eq. 1.10), the order of components is quite important. For example, the emission from the component farthest from the earth will get absorbed (or attenuated) by the components which are closer as the ray passes through them one by one. Freezing the spatial ordering was essential for us to be able to get a model which would be of practical use (see Sec. 4.2).

2.2.4 The Final Model

Our final model has N isolated isothermal clouds which have their order fixed by their indices (i.e. the first cloud is actually the first cloud that the ray will pass through). Each cloud has 4 parameters which almost completely determine its contribution towards the absorption and emission spectra - $T_{S,i}$, the spin temperature of the cloud, $\tau_{max,i}$, the peak optical depth of the cloud, $v_{c,i}$, the velocity at which the optical depth peaks, and $\sigma_{v,i}$, the velocity width (the σ factor) of the absorption profile.

The expected value for absorption at any velocity is given just by the sum of the optical depths of all the clouds at that particular velocity, which can be computed using the Gaussian function using the peak optical depth ($\tau_{max,i}$), the central velocity ($v_{c,i}$) and the velocity width ($\sigma_{v,i}$).

$$\tau_{expected}(v) = \sum_{i=1}^{N} \tau_i(v) = \sum_{i=1}^{N} \tau_{max,i} \exp(-\frac{1}{2}\frac{(v - v_{c,i})^2}{\sigma_{v,i}^2}) \tag{2.1}$$

The expected value for emission at any velocity is an iterative equation which computes the expected emission after the ray passes through each cloud one by one in the specified order.

$$T_{B,i}(v) = T_{B,i-1}(v)e^{-\tau_i(v)} + T_{S,i}(1 - e^{-\tau_i(v)}) \tag{2.2}$$

where $\tau_i(v)$, defined like in Eq. 2.1, is the optical depth of the i$^{\text{th}}$ component, and $T_{B,0} = T_{bg} = 0$.

Using these two expressions, we compute a joint χ^2 using the observed data and the errors on the data points

$$\chi^2 = \sum_{v=v_{\tau,min}}^{v_{\tau,max}} \frac{(\tau_{observed}(v) - \tau_{expected}(v))^2}{\sigma_\tau^2(v)} + \sum_{v=v_{T_B,min}}^{v_{T_B,max}} \frac{(T_{B,observed}(v) - T_{B,N}(v))^2}{\sigma_{T_B}^2(v)} \tag{2.3}$$

and try to minimize it for N clouds starting from 1 and then we keep adding more components till we hit an acceptable minimum reduced χ^2 (χ^2/DoF, where DoF, the number of degrees of freedom $= N_{data}^{abs} + N_{data}^{emi} - N - 1$) value close to 1.

An Alternative Model

We also tried an alternative model to take account of a few more parameters, but although this is likely to be somewhat more accurate physically, this could not be used as the final model for reasons discussed in Chapter 4.

This model uses an extra parameter for each cloud - the filling factor, f_i - which denotes the fraction of the emission beam filled by the particular cloud and hence is bounded between 0 and 1. The filling factor does not play any role in the absorption as the absorption beam is usually narrow enough to disallow any structure within the beamwidth. The emission, on the other hand, gets modified in this way

$$T_{B,i}(v) = (1 - f_i)T_{B,i-1}(v) + f_i T_{B,i-1}(v)e^{-\tau_i(v)} + f_i T_{S,i}(1 - e^{-\tau_i(v)}) \quad (2.4)$$

as only a fraction f of each cloud contributes to the attenuation and extra emission in the emission spectrum while the remaining part of it stays constant. We try to infer the value of the filling factor in our main model post-facto, using the differences between T_S and T_k.

Also, to take care of some other problems, we had to replace the parameter T_S by T_S/T_k which modifies every occurence of T_S to look like $(T_S/T_k) \times 121\sigma_v^2$, where $121\sigma_v^2$ is the kinetic temperature estimated from the velocity width of the line assuming only thermal broadening. This was only done to add constraints on f and T_S and it has no real effect on the above equation.

2.3 Methods

2.3.1 Minuit

Minuit is a minimization algorithm developed by James and Roos (1975)[11] and maintained by scientists in the CERN lab. For this work, we used a C-based version of this called C-Minuit which was adopted from a FORTRAN based Minuit code using CFORTRAN.

Minuit minimizes a given function over an n-dimensional parameter space. We used this routine to minimize the χ^2 function for our fits. It uses several different methods to get to the minimum. Once it finds a minimum in χ^2,

it calculates the intervals around the minimum beyond which χ^2 changes by 1, from which one can determine the 1-σ error values on the fitted parameters. Like almost all of the minimization algorithms, Minuit can converge to a local minimum instead of the global. But it can use methods like the Goldstein-Price method [12] to artificially remove the local minimum by Taylor expanding the function at the minimum and removing the second derivative term to get a new function whose minimum, if negative, is a better local minimum than the one already found. By repeating this, it can theoretically keep improving the local minimum and finally reach the global minimum, but there is no way to know when or whether it will reach it or not.

2.3.2 Anderson-Darling Test

The Anderson-Darling test (A-D test)[13] is a statistical test which determines whether a sample is taken from a particular distribution. It uses the Empirical Distribution Function (EDF) of the given data and compares it with the cumulative distribution function (CDF) of the given distribution to check for departures. For testing normality, while similar to the Kolmogorov-Smirnov test (K-S test), A-D test tries to weigh the tails as much as it weighs the central part, as opposed to the KS-test, which weighs the central region more than the tails. This makes A-D test one of the strongest tests for testing normality of a particular sample.[14] We have used this to determine whether the normalized residuals from the fits follow a standard normal distribution as a test, along with the χ^2 statistic, of whether the fit was good or not.

Chapter 3

Results

3.1 Pre-final results

Before implementing the final model, we worked with several approximate models as mentioned in Chapter 2. The independent Gaussian fits assumed no link between the absorption and emission spectra and treated them independently. They were preliminary fits to the spectra to estimate the approximate number of clouds one sees in the emission and absorption spectra. The joint Gaussian fits treated the absorption and emission spectra together, but assumed $\tau \ll 1$. The joint Gaussian fits were a step further and we believe that they give accurate estimates of parameters if the peak optical depth is $\ll 1$ as described in Sec. 1.4.1. Because the peak optical depth in all the datasets we used wasn't too high, the approximate models gave reasonable fits. We don't discuss these results here, as our final model makes no such assumptions and gives reasonable fits to the data.

3.2 Final Results

Fitting the 3 chosen spectra with our model gave us the fitted parameters which are listed in Tables 3.1, 3.2 and 3.3. Most headers denote parameters we discussed in our model. $N_{HI} = 1.83 \times 10^{18} \tau_{max} T_S \times \sigma_v \sqrt{2\pi}$ cm^{-2} indicates the column density of that particular component. In cold clouds where the filling factor lowers T_S from its actual value because the cloud does not fill the entire beam and the effective spin temperature output by the model is actually fT_S, T_k was used to estimate N_{HI} because $T_S = T_k$ for cold clouds. The parameter values marked with a '*' sign indicate that although the values output from Minuit are shown, the component is absent from the absorption

spectrum, which gives unrealistic values to those parameters. The fits are shown in Figures 3.1, 3.2 and 3.3.

The results from the individual sight-lines are described in detail in the following sub-sections.

3.2.1 PKS 0407-658

The sight-line towards PKS 0407-658 is a complex one with many components. The RMS values for T_B and τ are around 0.04 K with velocity resolution of 1.03 km/s and 0.001 with velocity resolution of 0.4 km/s, respectively. The fitted components in the sight-line towards PKS 0407-658 can be described as follows (in the order starting from the source to the observer):

1. This is a WNM component with $T_S \approx 1400K < T_k \approx 6800K$. Although it is not very strong in absorption, it is quite strong in emission. One of the dominant components in terms of $N_{HI} \approx 1.1 \times 10^{20}$ cm^{-2}.

2. This is the most dominant component in absorption. At a T_k of $\approx$ 90 K, its T_S of $\approx$ 2 K indicates that this component has a low filling factor (of around 0.02). Such cold clouds can be quite compact and the small filling factor is understandable.

3. A cloud slightly on the warmer side ($T_k \approx$ 850 K and $T_S \approx$ 600 K). Likely to be unstable as it is neither cold nor warm.

4. Very similar to the previous cloud, except somewhat weaker ($T_k \approx$ 700 K and $T_S \approx$ 500 K).

5. Another CNM cloud visible in both, absorption and emission, although not very strong in emission. T_k of 70 K and T_S of 10 K indicates a small filling factor of around 0.15 for this cold cloud.

6. Another cold cloud with $T_k \approx$ 85 K visible only in absorption. This cloud has an even smaller filling fraction of around 0.013, although the error is large.

7. A somewhat warm cloud at T_k around 460 ± 25 K, but has T_S of around 618 ± 47 K, which agrees at around 2.5-σ level. Likely to be unstable.

8. A warm cloud at around 4300 K just about visible in absorption, but quite strong in emission. The T_S of around 800 K agrees with theoretical expectations of $T_S < T_k$, but might suggest non-thermal broadening due to the large difference.

9. A warm cloud similar to the previous one, just twice as hot and weaker in both absorption and emission. This cloud seems to have $T_S \approx 600$ K, which is likely to be indicative of non-thermal broadening.

10. A warm cloud not seen in absorption at all. This causes the spin temperature to appear very high, but that is not the true spin temperature. Not much can be said about this cloud due to the large errors in the parameter estimates.

11. And finally a typical warm component with kinetic temperature of around 6000 K and spin temperature of around 3800 K. It is quite bright in emission, and is also visible in absorption, though it does not have very high optical depth. This is another dominant component in terms of $N_{HI} \approx 1.2 \times 10^{20}$ cm^{-2}.

The N_{HI} in the Warm Neutral Medium (components 1, 8, 9, 10 & 11) is 69.9$\pm$ 6.5% of the total N_{HI}, whereas those fractions for the CNM (components 2, 5 & 6) and the unstable medium (components 3, 4 & 7) are 16.7 ± 1.0% and 13.5 ± 2.1% respectively.

3.2.2 3C286

The sight-line towards 3C286 has very weak absorption and is an optically thin system. Also, the signal to noise ratio for this sight-line is lower than the other sight-lines. The RMS values for T_B and τ are around 0.08 K with velocity resolution of 1.03 km/s and 0.0003 with velocity resolution of 0.515 km/s, respectively. The fitted components in the sight-line towards 3C286 can be described as follows (in the order starting from the source to the observer):

1. A warm cloud at around 10000 K and has a T_S of around 2500 K. Appears to be the dominant component with $N_{HI} \approx 6 \times 10^{19}$ cm^{-2}.

2. A cold component at around 85 K with a low filling factor as indicated by the low T_S of about 10 K. The filling factor would be about 0.12.

3. Another cold component at around 105 K, with a filling factor of around 0.75 as indicated by the 80 K spin temperature.

4. One more cold component at around 250 K with a really tiny filling factor which cannot be estimated because of the large errors in the spin temperature due to its near absence in the emission spectrum.

5. A slightly warm component at around 650 K, but almost absent from absorption. T_S appears much larger, but the errors are also large, so there is no serious problem. Likely to be unstable.

6. Another warm component which is barely visible in both emission and absorption. Spin and Kinetic temperatures agree very well, but that is partly because the errors are large.

The N_{HI} in the Warm Neutral Medium (components 1 & 6) is $74 \pm 36\%$ of the total N_{HI}, whereas those fractions for the CNM (components 2, 3 & 4) and the unstable medium (component 5) are $12.9 \pm 2.1\%$ and $13 \pm 16\%$ respectively.

3.2.3 PKS 1814-637

This is a sight-line with very high signal to noise ratio. However, it appears to have many more components in emission where none are visible in absorption. RMS errors are around 0.044 K with velocity resolution of 1.03 km/s and 0.001 with velocity resolution of 0.4 km/s for T_B and τ, respectively. The fitted components in the sight-line towards PKS 1814-637 can be described as follows (in the order starting from the source to the observer):

1. This cold cloud is one of the two strong components in absorption. With a kinetic temperature of around 200 K and spin temperature of around 10 K, it seems to have a filling factor of about 0.05.

2. A warm wide component, possibly broadened non-thermally.

3. A well behaved somewhat warm component with $T_S \approx T_k \approx 700$ K. Likely to be unstable.

4. A cloud very similar to the previous one, but about 10 times stronger.

5. A warm component with $T_k \approx 3300$ K, which might mean it is unstable, and a T_S only slightly lower, which looks acceptable. This component is dominant in terms of $N_{HI} = 2.8 \times 10^{20}$.

6. A warm component at around 4500 K absent in absorption but quite strong in emission. Its absence in absorption gives rise to an unreliable estimate for T_S.

7. A very weak, but very wide component. Its kinetic temperature is unrealistic and cannot be trusted because of the poor signal to noise ratio for this component. Possibly unstable and non-thermally broadened,

or maybe an overlap of multiple weak wide components, but not much can be said due to the large errors.

8. The strongest component in absorption and quite strong in emission. It is quite cold with T_k of around 42 K and it has a T_S of around 25 K indicating a filling factor of around 0.6.

The N_{HI} in the Warm Neutral Medium (components 2, 6 & 7) is $26.0 \pm 2.7\%$ of the total N_{HI}, whereas those fractions for the CNM (components 1 & 8) and the unstable medium (components 3, 4 & 5) are $21.0 \pm 1.6\%$ and $52.9 \pm 2.1\%$ respectively.

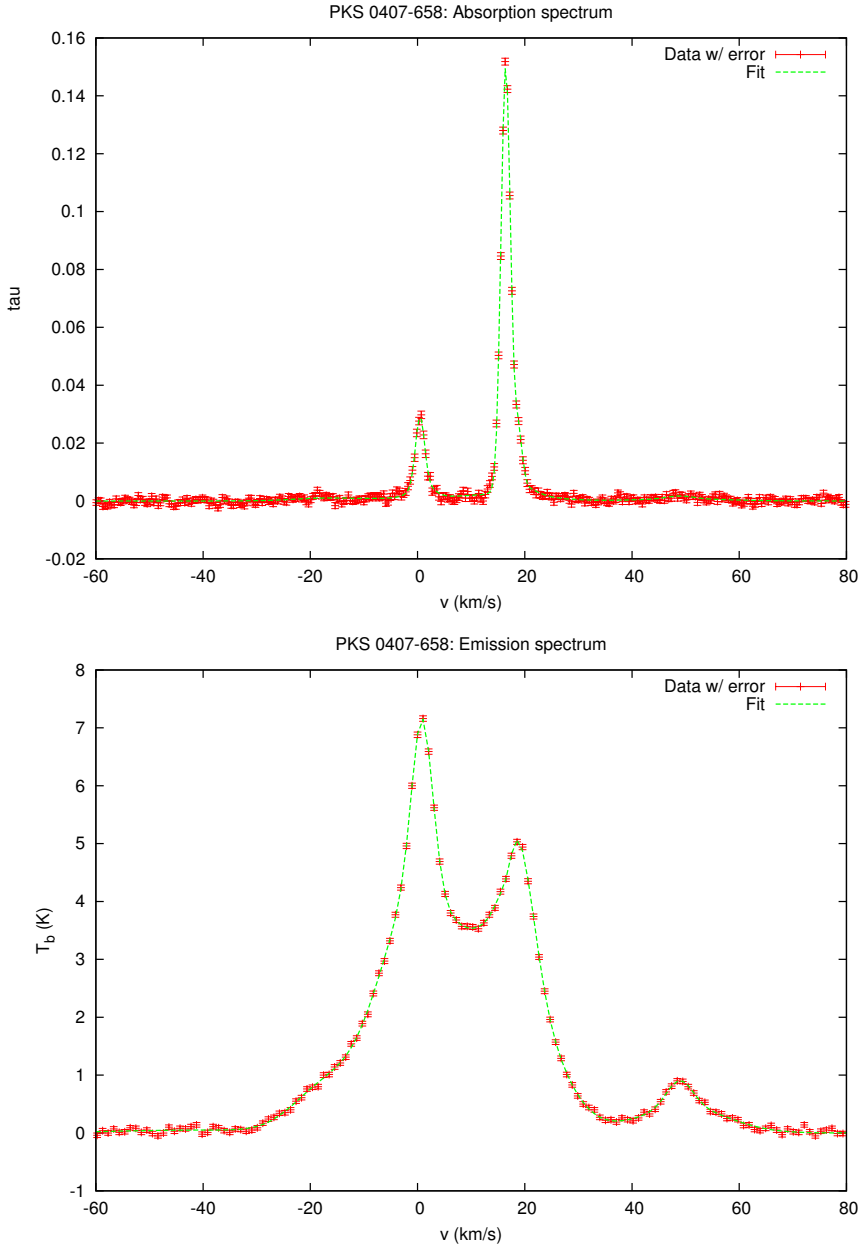

Figure 3.1: PKS 0407-658: The top and bottom panels show the absorption and emission spectra, respectively. The dashed line is the fit we obtained with our algorithm.

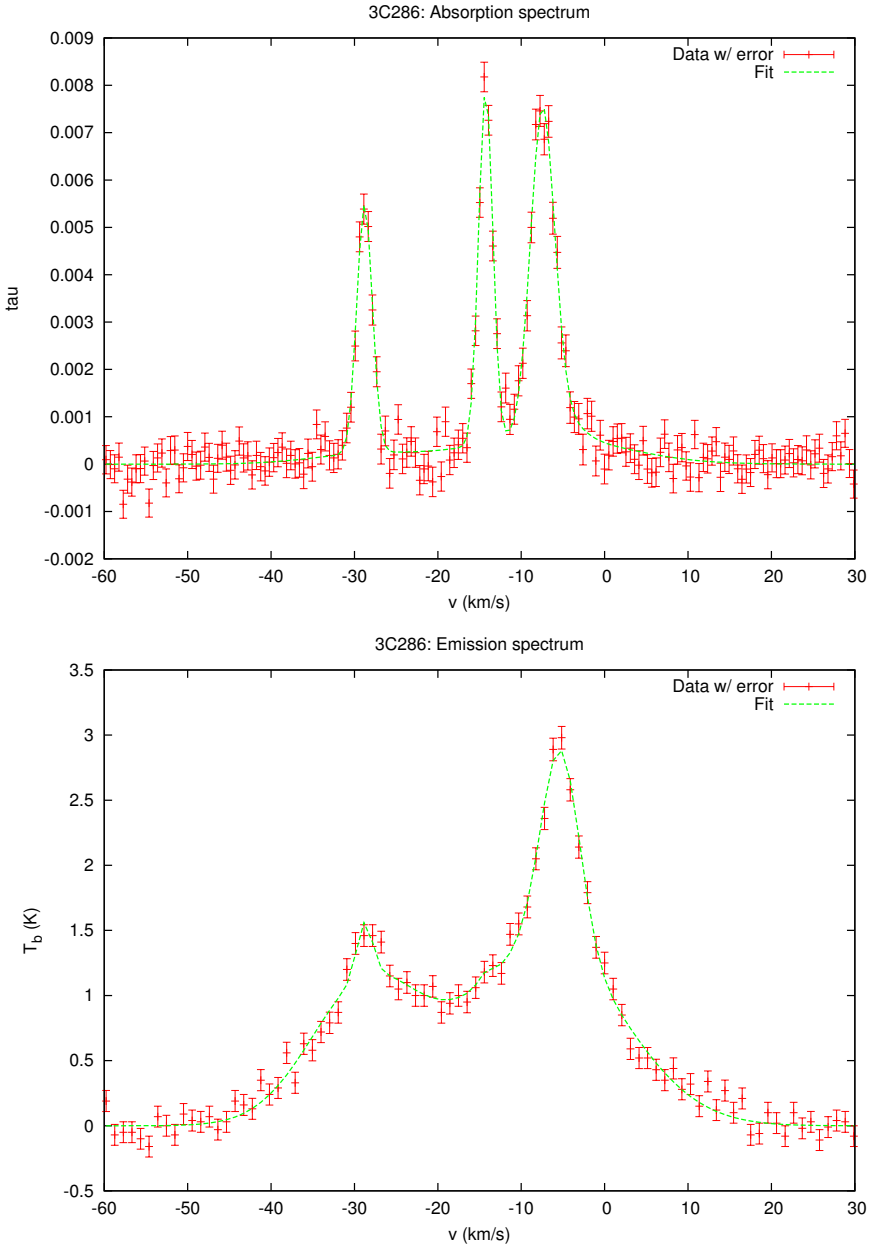

Figure 3.2: 3C286: The top and bottom panels show the absorption and emission spectra, respectively. The dashed line is the fit we obtained with our algorithm.

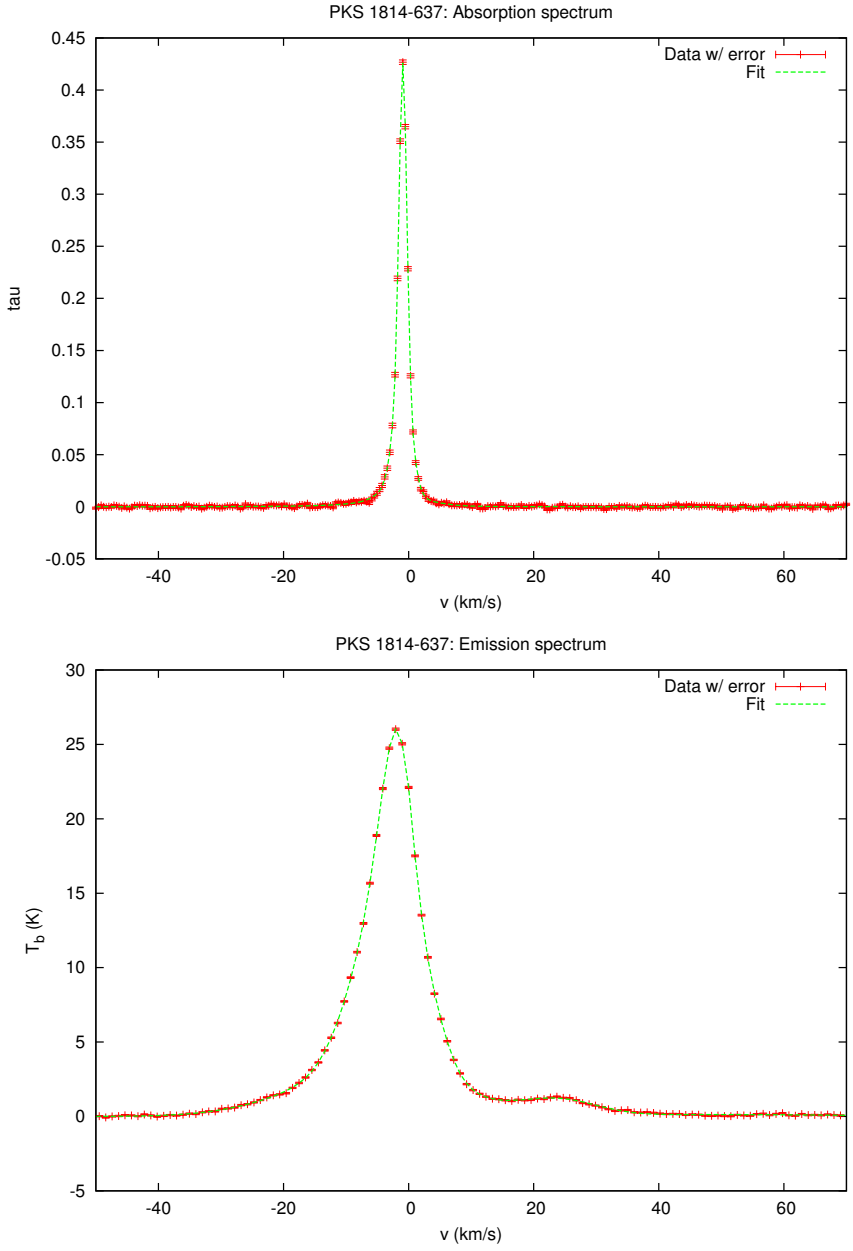

Figure 3.3: PKS 1814-637: The top and bottom panels show the absorption and emission spectra, respectively. The dashed line is the fit we obtained with our algorithm.

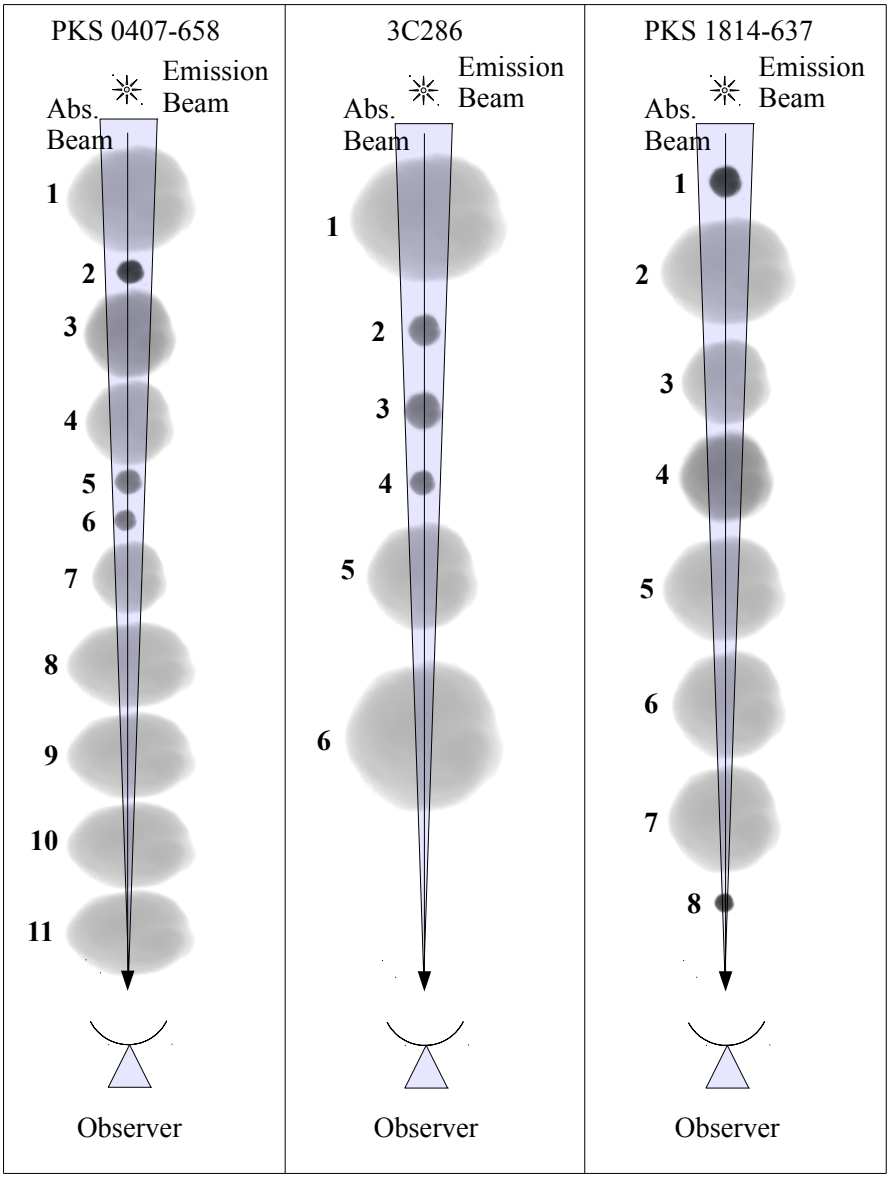

Figure 3.4: The illustrations of how the spatial arrangements of the clouds might look for the three sight-lines. The numbers next to the clouds indicate their indices in the model. The line leading from the background source to the antenna is the absorption beam and the triangular region around the absorption beam is the emission beam. The figure is not to scale and is only meant to help picturize the spatial distribution of the components along the sightline.

Table 3.1: The fitted parameters for PKS 0407-658

No.	τ_{max}	$\Delta(\tau_{max})$	T_S	ΔT_S	v_c	Δv_c	σ_v	$\Delta\sigma_v$	T_k	ΔT_k	N_{HI}	ΔN_{HI}
1	2.294e-03	8.163e-05	1435	50	16.26	0.29	7.52	0.20	6844	360	1.136e+20	6.378e+18
2	1.459e-01	7.956e-04	1.9	0.7	16.441	0.009	0.875	0.009	92.7	1.8	5.428e+19	1.700e+18
3	3.061e-03	3.061e-04	594	58	19.12	0.11	2.67	0.11	861	71	2.227e+19	3.249e+18
4	9.693e-04	2.620e-04	475	130	48.90	0.17	2.43	0.24	717	144	5.141e+18	2.050e+18
5	1.888e-02	9.221e-04	9.4	4.8	18.760	0.064	0.759	0.054	69.8	9.9	4.587e+18	1.003e+18
6	2.312e-02	8.996e-04	1.0	6.4	0.458	0.035	0.836	0.039	84.5	7.8	7.496e+18	1.089e+18
7	4.745e-03	3.639e-04	618	47	0.850	0.033	1.950	0.054	460	25	2.623e+19	2.925e+18
8	9.483e-04	1.196e-04	778	105	-17.25	0.57	5.98	0.40	4321	572	2.022e+19	3.985e+18
9	7.441e-04	1.359e-04	600	104	49.59	0.32	8.10	0.54	7942	1064	1.660e+19	4.320e+18
10	5.047e-08*	3.399e-08*	985931*	504216*	-41.15	6.88	14.7	6.8	26129	24246	3.354e+18	3.235e+18
11	1.023e-03	3.148e-05	3825	116	-0.64	0.19	6.94	0.21	5826	353	1.245e+20	6.577e+18

Table 3.2: The fitted parameters for 3C286

No.	τ_{max}	$\Delta(\tau_{max})$	T_S	ΔT_S	v_c	Δv_c	σ_v	$\Delta\sigma_v$	T_k	ΔT_k	N_{HI}	ΔN_{HI}
1	5.679e-04	1.298e-04	2443	516	-7.02	0.53	9.07	0.67	9954	1472	5.773e+19	1.847e+19
2	7.488e-03	2.370e-04	10.2	12.5	-14.262	0.029	0.843	0.035	86.0	7.2	2.491e+18	3.200e+17
3	5.254e-03	2.299e-04	78	17	-28.786	0.043	0.932	0.051	105.1	11.4	2.360e+18	4.011e+17
4	6.698e-03	2.442e-04	0.0	10.6	-7.458	0.074	1.436	0.067	250	23	1.101e+19	1.592e+18
5	4.443e-04	3.792e-04	3439	2914	-5.33	0.10	2.30	0.22	642	121	1.615e+19	1.948e+19
6	1.991e-04	1.017e-04	5402	2711	-28.56	0.46	6.68	0.39	5406	634	3.298e+19	2.369e+19

Table 3.3: The fitted parameters for PKS 1814-637

No.	τ_{max}	$\Delta(\tau_{max})$	T_S	ΔT_S	v_c	Δv_c	σ_v	$\Delta\sigma_v$	T_k	ΔT_k	N_{HI}	ΔN_{HI}
1	1.196e-01	6.178e-03	10.1	2.6	-0.971	0.018	1.271	0.027	195.6	8.2	1.364e+20	1.118e+19
2	9.581e-04	3.352e-05	3137	108	-5.93	0.20	12.31	0.15	18331	445	1.697e+20	8.603e+18
3	1.734e-03	2.603e-04	772	120	4.12	0.29	2.36	0.21	676	118	1.452e+19	3.383e+18
4	1.620e-02	4.498e-04	708	19	-1.849	0.049	2.543	0.033	782	20	1.339e+20	5.507e+18
5	3.785e-03	6.686e-05	3051	53	-3.413	0.085	5.242	0.058	3325	74	2.777e+20	7.517e+18
6	1.424e-06*	1.531e-07*	713946*	76545*	24.07	0.19	6.13	0.25	4547	366	2.859e+19	4.490e+18
7	4.101e-05	2.018e-05	3016	1488	50.3	3.0	20.00	0.90	48400	4339	1.135e+19	7.923e+18
8	2.874e-01	6.044e-03	24.78	0.55	-0.905	0.005	0.591	0.008	42.3	1.1	3.294e+19	1.506e+18

Chapter 4

Discussion

4.1 Distribution of HI among Cold, Warm and Unstable components

From the fits, we obtained the estimates for the fractions of the gas in the cold, warm and unstable neutral media. The results are summarised in Table 4.1.

The fractions of CNM along the three sight-lines are around 17%, 13% and 21%, which are not too different from each other. This means that the estimate for all the warm medium (including the unstable medium) of around 80 to 85% is inconsistent with the estimate of around 60% which Heiles & Troland (2003)[4] arrived at. They also estimated that at least 48% of the warm medium is unstable, meaning that about 29% of all the HI is unstable. We have results inconsistent with this estimate as well and the fractions of the unstable medium are very different for the three sight-lines. This might indicate the existence of some spatial structure on the galactic scale for the unstable medium.

Table 4.1: Fractions of gas in the Cold, Warm and Unstable Media along the three sight-lines

Sight-line	WNM	CNM	Unstable Medium
PKS 0407-658	$69.9 \pm 6.4\%$	$16.7 \pm 1.0\%$	$13.5 \pm 2.1\%$
3C286	$74 \pm 36\%$	$12.9 \pm 2.1\%$	$13 \pm 16\%$
PKS 1814-637	$26.0 \pm 2.1\%$	$21.0 \pm 1.6\%$	$52.9 \pm 2.1\%$

4.2 Spatial ordering and shuffling of components

Heiles and Troland (2003)[5] tried to include spatial ordering in their codes. Because they had two different classes of clouds - CNM and WNM - they had to solve for the spatial ordering after they had first frozen the number and properties of the different components along each line of sight. This meant that their problem was about shuffling the spatial positions of the clouds and look for the best arrangement. However, this problem has a factorial order in the number of cold components with non-negligible optical depths which again gets multiplied by an exponential order in the remaining clouds. This makes it computationally intractable. Heiles and Troland tried to reduce the latter to get only 3 distinct cases of all of the WNM being behind CNM, all of the WNM being in front of the CNM and a middle case where roughly half of the WNM is behind the CNM and half of it is in front. Even then, the order of their shuffling algorithm was $O(N_x!3^{K_x})$ where N_x is the number of overlapping cold components (so that the attenuation matters) and K_x is the number of WNM clouds behind the cold clouds. Even with the reduced number of components, this algorithm would take an unrealistically long time to run.

We were trying a similar algorithm, where we would shuffle the initial conditions and then proceed to fit the data and find the best fit among all the orderings. But we realized that including a fitting routine along with a factorial order algorithm would really have been unrealistic computationally and it would be better to take a completely different approach.

That was when we realized that the ordering was a problem because we were considering the cold and warm clouds differently. However, in reality, the physics is the same for both kinds of clouds and including a single model for both kinds of clouds would help with freezing the spatial ordering (as we have done now; see Sec. 2.2.4), and would also be physically more accurate. In such a case, if the minimization algorithm is robust enough, shuffling the initial conditions would make no difference as the order is inbuilt in the fitted function and it will always lead to the same global minimum, thus removing the need of shuffling and making the algorithm much much faster.

However, finding the global minimum is difficult for any algorithm and there is no way to know that the minimum you have reached is a global minimum. MINUIT is one of the better algorithms for minimization and it includes a routine to implement the Goldstein-Price method[12] which artificially removes the local minimum that the algorithm has found and looks for a new minimum, which, if it is lower than the previous local minimum,

is a better solution to the problem. We have tried to implement this in our code, but again, like all global minimization algorithms, there is no way to know if the minimum reached is indeed the global minimum.

4.3 Need for a filling factor

The absorption and emission spectra of PKS 0407-658 show a peculiar feature which necessitates the addition of a filling factor. The absorption spectrum has a strong absorption peak at around +16 km/s. Corresponding to it, however, there appears to be little or no contribution from that component in the emission spectrum. Given its optical depth of 0.14 and a minimum possible spin temperature of about 20 K, it was expected to have a component in emission which would be at least 2.8 K strong. However, the absence of any such component in emission implies that we can put constraints on the angular extent of the absorbing cloud by using an additional beam filling factor which would determine the contribution of the absorption clouds to emission in terms of how much of the telescope beam they fill. With the fits from our model, we found that the component had an effective spin temperature of around 1.9 K, which is about 2% of the kinetic temperature (which is around 92 K and the actual spin temperature is also expected to have the same value), meaning that the derived filling factor is about 0.02.

4.4 f-T_S Degeneracy

When the filling factor is included in the model as a free parameter modifying the brightness temperature (see the alternative model in Sec. 2.2.4), some more problems arise. When the filling factor is very small, its effect on the background emission is negligible. In such a case, the only significant term which changes the brightness temperature is $fT_S(1 - e^{-\tau})$. Here, f and T_S appear together and only their product contributes to the equation. Also, these two parameters do not directly contribute to the absorption. This leads to a degeneracy in the values of f and T_S where the two parameters may take a large range of values while keeping the product constant. For example, a cloud with filling factor 10^{-3} and T_S of 20 K and another with filling factor 10^{-6} and T_S of 20000 K, are almost equivalent. This often leads to large error estimates for these two parameters when such a condition arises.

4.5 Problems with Limits

To get around the f-T$_S$ degeneracy, T_S was replaced by a T_S/T_k factor in which the T_k is determined by the velocity width of the fitted Gaussians and T_S is forced to stay in the range of $0.05T_k$ and T_k for reasons mentioned in Sec. 1.5. However, this causes two parameters to be bounded inside limits - T_S/T_k and f (which is bounded between 0 and 1) - and in most cases the parameters are very close to their upper limits ($T_S = T_k$ is quite common for cold clouds and $f = 1$ is quite common for warm ones). This led to too many parameters getting too close to their limits which causes the errors in these parameters to be highly unreliable as the minimum reached may not correspond to a true local minimum in the χ^2 profile. So we switched back to the previous model without f and T_S/T_k, and decided to interpret the filling factors post-facto from the (somewhat) unconstrained fits.

4.6 Further Possibilities

We have only worked with 3 data sets here, but there are a lot more data sets available with varying levels of complexity and trying to get fits using our model would help us to be able to describe those sight-lines as well. Also, the large number of available data sets could be used to get the distributions of properties of the clouds, which will help us understand the distribution of clouds in the ISM. It would also be a good way to test whether the currently believed model of the coexistence of two distinct CNM and WNM phases is correct.

Another interesting exercise would be to compare the spatial structure of the ISM obtained from the fits to the current understanding of the spatial structure of our galaxy to build on our knowledge of the ISM.

To address the problem of finding the global minimum, one could try to use Monte-Carlo methods or grid methods to seek the true global minimum, which would then make this model even better at estimating the physical properties of the components of the ISM. However, given the large number of parameters and data points, those methods are likely to be highly computationally expensive.

Chapter 5

Summary

To summarize, taking into account the radiative transfer equation, we developed a new model to fit the absorption and emission spectra jointly by minimizing the joint χ^2. With the three fits obtained from the three data sets we used, we were able to describe the components in each sight-line in detail.

We also have estimates of the fractions of interstellar HI in the different phases and we found a significant fraction of HI in the unstable phase in two sight-lines, which somewhat contradicts the two phase model of interstellar HI and makes way for an unstable medium with typical values of temperature in between those of the warm and the cold neutral media. This result qualitatively agrees with the result that Heiles & Troland (2003)[4] arrived at. However, the fraction of gas in the unstable medium varies a lot between the three sight-lines. But we studied only three sight-lines and the results would need to be obtained for many more such sight-lines to be able to comment on the actual distribution of interstellar HI among these components.

We also have a possible alternative model, the implementation of which was not possible for us, but if used in future studies, it could prove to be effective.

References

[1] S. R. Kulkarni, C. Heiles, Neutral hydrogen and the diffuse interstellar medium, 1988, pp. 95–153.

[2] G. B. Rybicki, A. P. Lightman, Radiative processes in astrophysics, 1979.

[3] N. Kanekar, R. Subrahmanyan, J. N. Chengalur, V. Safouris, The temperature of the warm neutral medium in the Milky Way, Monthly Notices of the RAS 346 (2003) L57–L61. arXiv:arXiv:astro-ph/0310761, doi:10.1111/j.1365-2966.2003.07333.x.

[4] C. Heiles, T. H. Troland, The Millennium Arecibo 21 Centimeter Absorption-Line Survey. II. Properties of the Warm and Cold Neutral Media, Astrophysical Journal 586 (2003) 1067–1093. arXiv:arXiv:astro-ph/0207105, doi:10.1086/367828.

[5] C. Heiles, T. H. Troland, The Millennium Arecibo 21 Centimeter Absorption-Line Survey. I. Techniques and Gaussian Fits, Astrophysical Journal, Supplement 145 (2003) 329–354. arXiv:arXiv:astro-ph/0207104, doi:10.1086/367785.

[6] P. M. W. Kalberla, W. B. Burton, D. Hartmann, E. M. Arnal, E. Bajaja, R. Morras, W. G. L. Pöppel, The Leiden/Argentine/Bonn (LAB) Survey of Galactic HI. Final data release of the combined LDS and IAR surveys with improved stray-radiation corrections, Astronomy and Astrophysics 440 (2005) 775–782. arXiv:arXiv:astro-ph/0504140, doi:10.1051/0004-6361:20041864.

[7] D. Hartmann, W. B. Burton, Atlas of Galactic Neutral Hydrogen, 1997.

[8] E. M. Arnal, E. Bajaja, J. J. Larrarte, R. Morras, W. G. L. Pöppel, A high sensitivity Hi survey of the sky at $\delta \leq -25^o$, Astronomy and Astrophysics, Supplement 142 (2000) 35–40. doi:10.1051/aas:2000134.

[9] E. Bajaja, E. M. Arnal, J. J. Larrarte, R. Morras, W. G. L. Pöppel, P. M. W. Kalberla, A high sensitivity HI survey of the sky at $\delta \leq$ -25 deg . Final data release, Astronomy and Astrophysics 440 (2005) 767–773. arXiv:arXiv:astro-ph/0504136, doi:10.1051/0004-6361:20041863.

[10] R. Braun, N. Kanekar, Tiny H I clouds in the local ISM, Astronomy and Astrophysics 436 (2005) L53–L56. arXiv:arXiv:astro-ph/0505055, doi:10.1051/0004-6361:200500122.

[11] F. James, M. Roos, Minuit - a system for function minimization and analysis of the parameter errors and correlations, Computer Physics Communications 10 (1975) 343–367. doi:10.1016/0010-4655(75)90039-9.

[12] A. Goldstein, J. Price, An effective algorithm for minimization, Numerische Mathematik 10 (3) (1967) 184–189.

[13] T. W. Anderson, D. A. Darling, Asymptotic theory of certain goodness of fit criteria based on stochastic processes, Annals of Mathematical Statistics 23 (1952) 193–212.

[14] M. A. Stephens, EDF statistics for goodness of fit and some comparisons, Journal of the American Statistical Association 69 (347) (1974) 730–737. arXiv:http://www.tandfonline.com/doi/pdf/10.1080/01621459.1974.10480196, doi:10.1080/01621459.1974.10480196. URL http://www.tandfonline.com/doi/abs/10.1080/01621459.1974.10480196